

Cascade Modeling of the Measuring System Used to Assess S-Parameters of Anchor Rods on Power Transmission Lines Guyed Towers

V. L. Tarragô¹ , M. T. de Melo¹ , Lauro R. G. S. Lourenço Novo¹ , Douglas C. P. Barbosa¹ ,
Marcelo S. Coutinho¹ , Luiz H. A. de Medeiros¹ , Marcelo M. Alves¹ ,
Renan G. M. dos Santos¹ , Henrique B. D. T. Lott Neto² , Paulo H. R. P. Gama³ 

¹Federal University of Pernambuco, Recife, Brazil, viniciuslealt@icloud.com, marcostdemelo@gmail.com,
lauronovo@yahoo.com.br, douglas.pbarbosa@ufpe.br, msacou@gmail.com, luiz.medeiros@ufpe.br,
marceloalves87@gmail.com, renangsantos@icloud.com

²Sistema de Transmissão Nordeste S.A., Recife, Brazil, hlott@stnordeste.com.br

³Instituto Avançado de Tecnologia e Inovação, Recife, Brazil, paulogama@versattus.com.br

Abstract— The structural condition of the cable-stayed towers anchorage on power transmission lines requires constant monitoring. Maintenance routines must be able to identify faulty anchor rods and substitute them to avoid tower collapses and power delivery interruptions. Modern statistical diagnostic systems based on machine learning requires the generation of several distinct rod sample signals to be trained, which is a time-consuming process in typical electromagnetic solvers. Aiming to generate samples in a feasible time span, this paper presents a modeling strategy based on the cascade analysis of the transmission line composed by the anchor and the reference rods, interconnected by a dedicated high-frequency connector. Each distinct transmission line part is modeled by a quadrupole as a partial ABCD matrix. The complete response for each experimental setup is obtained from the cascaded-multiplying of the partial matrices. The proposed modeling proved to be accurate and provides a faster way to obtain the S-parameters from distinct faulty rods if compared to the traditional methodologies using electromagnetic tools.

Index Terms— ABCD matrices, Anchor rods, Electromagnetic modeling, S-parameter, Transmission line.

I. INTRODUCTION

Cable-stayed structures such as the VX6-type towers have been broadly applied in power transmission lines due to their relative low cost if compared to the self-supporting towers for the same service. However, a cable-stayed tower has a higher risk of collapse, because its stability and balance depend on anchor rods, which are more likely to fail than the heavy metallic structure of the self-supporting towers. A catastrophic failure of a single transmission line tower could cause thousands of consumers to run out of electricity and penalize the transmission company to the payment of expensive penalties to government and regulatory agencies. Therefore, it is mandatory to perform preventive maintenance on the anchor rods in order to prevent the towers from falling down. Currently, the maintenance is done by visual inspection of the anchor rods, which is an expensive and

time-consuming process, since the rods are normally buried and need to be uncovered from soil for visualization [1], [2].

Previous work has suggested a non-destructive method of inspecting these rods through frequency domain reflectometry, using a vector network analyzer (VNA) and machine learning tools [1]–[7]. Although machine learning tools have demonstrated excellent performance on corrosion diagnosis, they depend on expressive databases composed by signals relative to several rods conditions for model training. Creating a database from thousands of the required EM simulations takes a long time, as the differences in dimension of the elements of the system makes the simulation model quite complex and time-consuming to solve numerically. On the other hand, trying to provide a database through measurements can be even more costly as it requires a well-trained staff performing acquisitions in the remote and hard accessing places in which the power transmission lines are usually located.

Computer analytical calculations are generally faster than the traditional modeling by numerical methods which uses iterations of variables and finite elements from simulations [8], [9]. Modelling by high-fidelity computer simulations have already been done for elements such as eye bolts, anchor rods, insulators, transducers and cables [10]–[12]. Table I presents a comparison of the general characteristics of several methods already proposed in literature to model transmission line structures to design detecting systems.

TABLE I. GENERAL CHARACTERISTICS FROM SIMILAR SYSTEMS AND THE PROPOSED ONE.

Reference	Modelling Method	Structure analyzed	HF connector	Fault diagnosis	Field application
[2]	EM simulation	Anchor rods	Yes	Yes	Yes
[3]	EM simulation	Anchor rods	Yes	Yes	No
[10]	Equivalent circuit + EM simulation	Eye bolts	Yes	Yes	Yes
[11]	Reflection coefficient analysis + EM simulation	Transducers	No	No	Yes
[12]	Reflection coefficient analysis	Cables	No	Yes	Yes
Proposed method	Cascade analysis + EM simulation	Anchor rods	Yes	Yes	Yes

Aiming at optimizing the time for obtaining simulated signals from different conditions of rods, this paper proposes a modeling of the anchor rod and its high-frequency connection system through quadrupoles. The entire scheme was divided in different parts according to the structural features, for instance, presence of the connector, faultless or faulty anchor rod sections, and so on. Every part was

modeled as a quadrupole, making possible to join the solutions and find an equivalent response of the system in a cascade analysis.

II. METHODOLOGY

In this paper, two different arrangements were modeled according to the test environment, namely, laboratory and experimental field setups. The laboratory setup consists of two rods in parallel (anchor and reference rods) connected to the high-frequency connector MDSC (Microwave Device of Support and Connection). The MDSC is a dedicated device developed by the author's research group to interface the VNA, and the transmission line composed by the rods, as a low loss connector.

A. Laboratory setup

The laboratory setup was performed with rods 1.0 to 3.0 m long due to space and safety restrictions to manipulate them indoors. However, the proposed modelling can be applied to any rod lengths. In the laboratory setup, each different part of the transmission line is represented by a partial ABCD matrix. The complete quadrupole model is obtained by interconnecting the partial matrices in a cascade analysis. Figure 1 presents examples of faulty (a) and faultless (b) rods of the laboratory setup.

In the faulty system of Fig. 1 (a), part 1 represents a transmission line part (TLP) which contains the MDSC. Part 1 has been simulated electromagnetically using the Ansys HFSS software [13]-[14], widely employed for high-frequency applications [15]-[17]. Part 2 is composed by the TLP formed by the faultless anchor rod and the reference one. Part 3 represents a TLP whose length is defined by the extension of the fault on the anchor rod. Finally, part 4 has similar geometry of part 2, although, it presents a different length and is terminated by the free space. On the other hand, the setup of the faultless anchor rod is shown in the Fig. 1 (b), and it has only two parts: Part 1 relative to the MDSC, as previously explained, and Part 2 which represents a TLP for a faultless anchor rod ended by the free space.

The lengths for each part are represented by L_1 , L_2 , L_3 , and L_4 . The length of part 1 is L_1 which is relative to the high frequency connector, and therefore it remains unchanged regardless of the specific configuration. The lengths L_2 , L_3 and L_4 can take any value, depending on the length of the rod, the position, and the size of the fault. For example, the results presented in this paper used L_2 values ranging from 50 to 290 cm, L_3 ranging from 10 to 20 cm, and L_4 ranging from 40 to 90 cm.

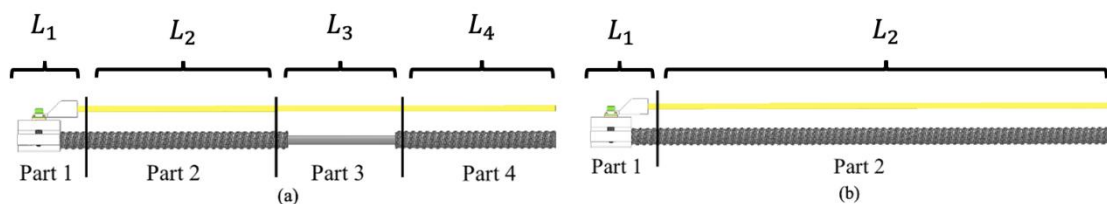


Fig. 1. Laboratory setup for two different conditions of the anchor rod. (a) faulty. (b) faultless.

B. Field setup

The field setup was modeled as shown in Fig. 2, and the entire model can be divided in two parts. Part 1 represents the MDSC and part 2, the non-uniform transmission line, composed by the anchor and reference rods, which may or may not exhibit a fault. Parts 1 and 2 were modeled using the Ansys HFSS EM software, whereby the S-parameters were obtained to determine the respective ABCD matrices. The matrix of part 1 is the same regardless the rod setup, therefore, its simulation is just run one time.

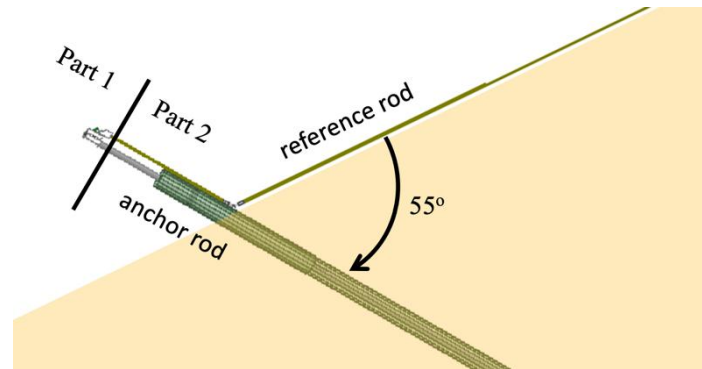


Fig. 2. Parts of the experimental field setup.

Fig. 3 depicts both the basic scheme of a cable-stayed VX6 Tower (a), and a photograph of an actual field measurement (b). The experimental field setup presents a 55 degrees-angular displacement between the anchor and reference rod, since only the anchor is buried in soil, as detailed in Fig. 2.

From the conversion of the responses of each part from S-parameters to ABCD parameters, it is possible to obtain the overall result by multiplying of the individual ABCD matrices [18].

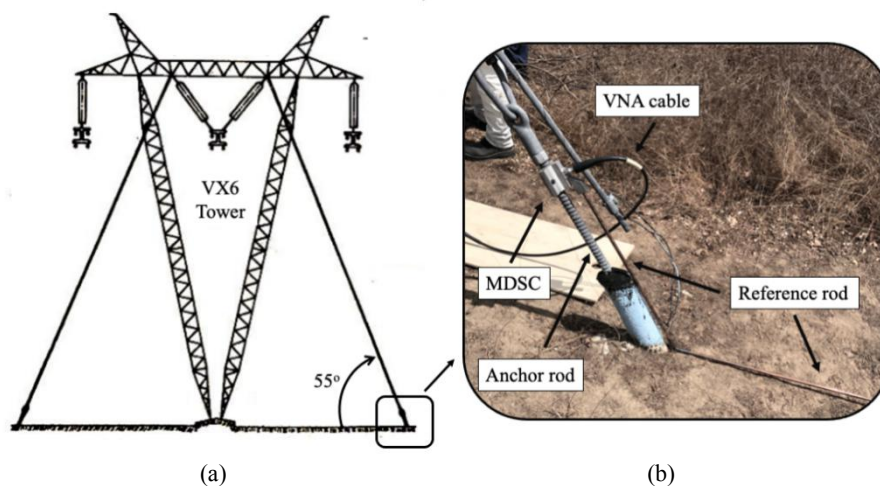


Fig. 3. Field setup. (a) Cable-stayed VX6-type tower assembly. (b) Photography of the experiment on field tests.

C. MDSC Modeling

The MDSC was modeled using Ansys HFSS software. Discrete 50Ω-ports were inserted at MDSC

input (VNA connection, port 1), and at its output (both anchor and reference rods connection, port 2) to get the matrix of S-parameters. Fig. 4 (a) shows the simulation design in HFSS, and Fig. 4 (b) presents the respective magnitude of S-parameter responses. In lower frequencies, S11 is equal to S22 and S12 is equal to S21, once such parameters are obtained from a passive device whose electrical properties remain unchanged regardless the direction of the electromagnetic wave propagation [10].

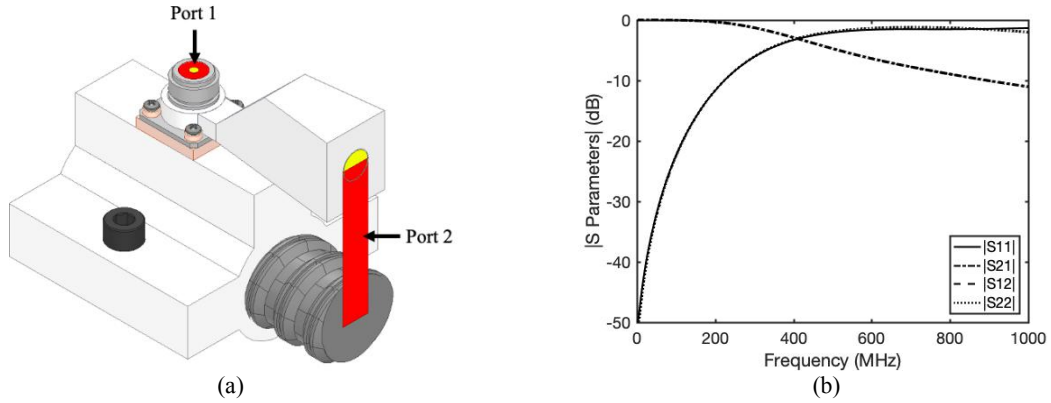


Fig. 4. MDSC simulation. (a) 3D HFSS EM model. (b) S parameters responses.

Phase information, although not presented in Fig. 4, was used for converting the S-parameters to ABCD matrix. The chosen frequency range for the MDSC simulation compatible to the one used to calibrate the measuring instruments in the field, which goes from 2 MHz to 1 GHz.

D. Laboratory Setup Modeling

The transmission line composed by both reference and anchor rods was modeled based on the Traveling Wave Theory where they were represented by a copper 11mm-diameter and a steel 34mm-diameter cylinders, respectively. These are the typical diameter values chosen for anchor rods in real field applications. The geometric and electromagnetic parameters from the cross section of the two-rod transmission line determine the RLGC electric parameters.

Equations (1), (2) and (3) determine the RLGC parameters, where D is the distance between the reference and anchor rods, and d_1 and d_2 their respective diameters, as shown in Fig. 5. The parameter G can be considered null because the conductors are properly spaced and insulated from each other [18], [19].

$$L = \frac{\mu}{2\pi} \cosh^{-1} \left(\frac{4D^2 - d_1^2 - d_2^2}{2d_1d_2} \right) \quad (1)$$

$$C = \frac{2\pi\epsilon}{\cosh^{-1} \left(\frac{4D^2 - d_1^2 - d_2^2}{2d_1d_2} \right)} \quad (2)$$

$$R = \sqrt{\frac{f\mu}{4\pi} \left(\frac{1}{d_1\sqrt{\sigma_1}} + \frac{1}{d_2\sqrt{\sigma_2}} \right)} \quad (3)$$

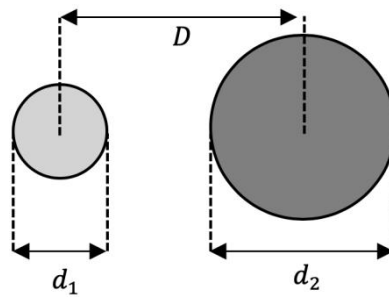


Fig. 5. Cross section of the transmission line composed by the anchor (right) and reference (left) rods [19].

The parameters L , C , and R represent the inductance, capacitance, and resistance, respectively per meter, f is the signal linear frequency, and σ_1 and σ_2 are the electric conductivities of the reference (copper) and the anchor (steel) rods, respectively.

To validate the two-rod transmission line model of equations (1), (2) and (3), as well as the approximation of the anchor rod by a cylinder, a simulation with an anchor rod was performed in software Ansys HFSS and the result was compared with the calculations. Fig. 1 (b) shows the model of the pair of rods (part 2).

Fig. 6 presents the simulated and calculated results of $|S_{11}|$ and $|S_{12}|$ from RLGC parameters, for 1-meter and 3-meter faultless rods until 400 MHz.

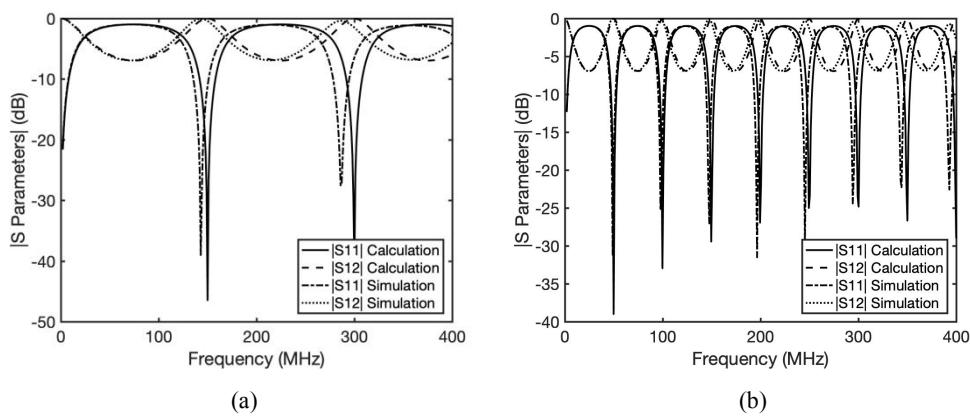


Fig. 6. Simulated and calculated results from the two-rod transmission line for two lengths. (a) 1-meter. (b) 3-meter.

The frequency range was chosen based on the main resonances of the system, as the pair of rods presents resonance frequencies based on the length of the transmission line. Since this transmission line is symmetric, the parameters $|S_{22}|$ and $|S_{21}|$ are the same as parameters $|S_{11}|$ and $|S_{12}|$, respectively [10]. There is a great similarity between the simulated and calculated results, showing that the presented model is reliable for representing faultless two-rod transmission lines. The characteristic impedance of the two-rod transmission line setup resulted in 210Ω . In this case, simulations and calculations have used a 50Ω -port at each termination of the transmission line, featuring a 2-port network.

Similarly, the faulty two-rod transmission line was modeled from equations (1), (2) and (3), considering that the reference rod continues faultless, and the anchor rod suffers a reduction on its d_2 diameter to represent a structural fault e.g. a corrosion process, as modeled in Fig. 1 (a). The obtained RLGC parameters were converted to be used in an ABCD matrix for each part of the transmission line, and after that these matrices were multiplied to obtain the complete ABCD matrix.

Referring to Fig. 1 (a), $ABCD_{tl}$ is the equivalent ABCD matrix of the complete transmission line, $ABCD_{p2}$ is the ABCD matrix of the part 2, $ABCD_{p3}$ is the ABCD matrix of the part 3, i.e., the section of the transmission line relative to the fault part, and $ABCD_{p4}$ is the ABCD matrix of the part 4.

Equation (4) presents the matrix cascade calculation to obtain the complete ABCD matrix.

$$ABCD_{tl} = ABCD_{p2} \times ABCD_{p3} \times ABCD_{p4} \quad (4)$$

Finally, in order to obtain the complete response matrix ($ABCD_{complete}$) of the laboratory setup, the matrix $ABCD_{mdsc}$ was multiplied by the $ABCD_{tl}$, as defined in (5).

$$ABCD_{complete} = ABCD_{mdsc} \times ABCD_{tl} \quad (5)$$

Fig. 7 shows a good agreement between the calculated (equation (4)) and simulated (HFSS) results for the faulty two-rod transmission line validating the cascade analysis up to 400 MHz.

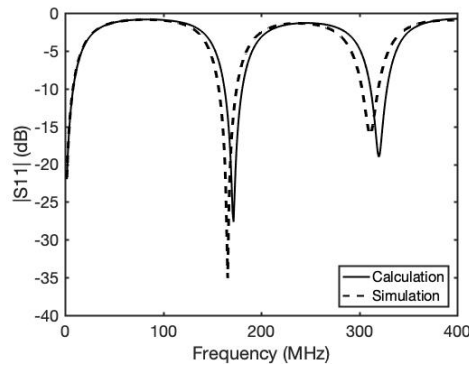


Fig. 7. Simulated and calculated results from a faulty 1-meter two-rod transmission line.

E. Field Setup Modeling

There is a great complexity in analytically modeling the field setup, presented in Fig. 2, due to the 55 degree-angle between the anchor and reference rods which represents a non-uniform transmission line.

As the MDSC quadrupole is previously obtained, it is possible to simulate part 2 of the transmission line presented in Fig. 2 to obtain the reflection coefficient at its input. Fig. 8 presents a schematic diagram corresponding to equation (6), in which the quadrupole of S-parameters represents the MDSC, Γ_L is the reflection coefficient of part 2, and Γ_{in} is the reflection coefficient of the complete system. In this case, Γ_{in} is equal to the S_{11} of the complete system since measurements are made with only one port because the end of the anchor rod is buried. So, S_{12} , S_{21} and S_{22} of the complete system

are null because it is a 1-port network. [1], [2], [18].

$$\Gamma_{in} = S_{11} + \frac{S_{12}S_{21}\Gamma_L}{1 - S_{22}\Gamma_L} \quad (6)$$

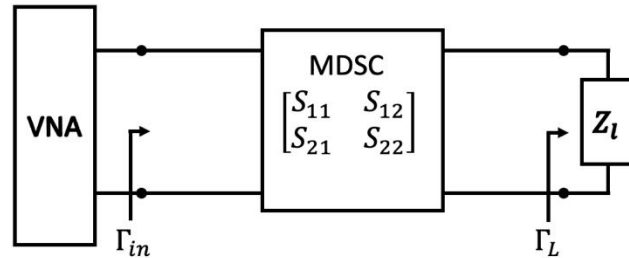


Fig. 8. Schematic diagram from equation (6).

Anchor rods in the field setup are usually 6-meter long and MDSC has few-millimeter-long pieces. Joining elements with different orders of magnitude in length increases the difficulty of the mesh process and makes the EM simulation to take a long time [9].

III. RESULTS AND ANALYSIS

Measurements are made with only one port even for the laboratory setup, because the only way to perform measurements with two ports in laboratory is to insert another MDSC at the end of the transmission line. It can be an impracticable task which depends on the length of the anchor rod, and VNA cables are usually few-centimeters long. Furthermore, in the real field situation, the end of the rod is inaccessible because it is buried in the soil.

Therefore, to allow the comparison between the modeling and the measurement results (for the laboratory setup), it is necessary to model the one-port experiment setup. For this, it is necessary to know the impedance or the reflection coefficient at the end of the transmission line. A simulation can be performed to obtain the reflection coefficient at the end of the line and to use it in equation (6) as Γ_L . In this case, the S-parameter quadrupole would be obtained from the conversion of the $ABCD_{complete}$ matrix.

A open end section of the transmission line with $L_{end} = 80$ cm length was simulated and its Γ_L was

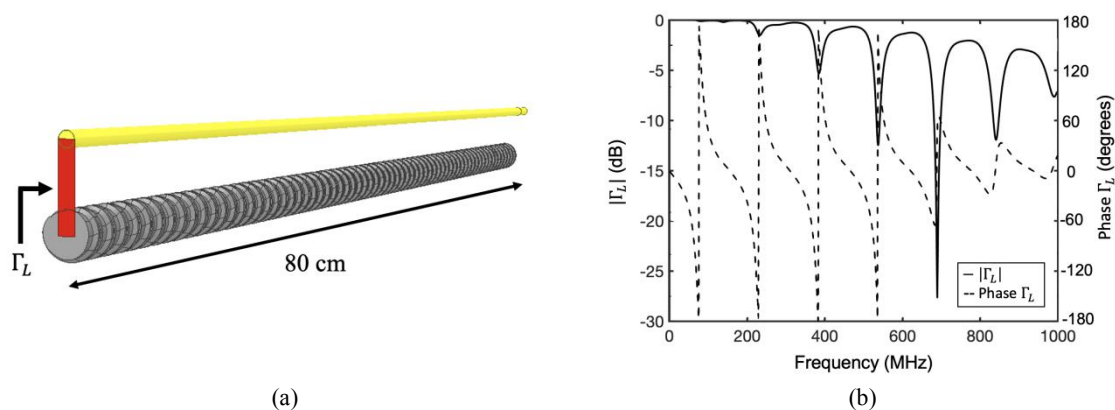


Fig. 9. Simulation setup (a) and the Γ_L response (b) of the 80 cm open transmission line section.

obtained. This end section is a simulation artifice that represents the termination of the two-rod transmission line and replaces the previous 50Ω -port, turning the 2-port network into a 1-port network. Then, the length of part 4 of Fig. 1 (a) must now take the value of $L_4 - L_{end}$ and the length of part 2 of Fig. 1 (b) assumes $L_2 - L_{end}$. Due to limitations of the software used, the shortest length that guarantees the correct propagation mode at the termination of the TL is $L_{end} = 80$ cm.

Fig. 9 (a) shows the simulation setup and Fig. 9 (b) the magnitude and phase of Γ_L response for this transmission line section up to 1 GHz. Therefore, it is possible to use this Γ_L in equation (6) for modeling any anchor rod condition (if the fault is not located along the length of the end section). This transmission line end section is common to all anchor rod conditions in the laboratory setup, and it doesn't need to be simulated again, as it happens with the MDSC.

Fig. 10 shows a comparison between the laboratory setup responses of the measurement from the VNA, the simulation from Ansys HFSS and calculation from the proposed method, for 2-meter faultless (a) and faulty (b) anchor rods. The fault on the faulty rod is placed 50 cm from the MDSC and corresponds to a 17 mm reduction in the diameter.

The results in Fig. 10 presents better correlation at lower frequencies. As the frequency is increased, the displacement between the resonance frequencies also increases for the measured result compared to the calculated and simulated ones. However, it is noted that the results show the same number of resonant frequencies up to 600 MHz, showing that the proposed method for modeling the anchor rods in the laboratory setup is as useful as the 3D electromagnetic simulation, but much more efficient in terms of computational efforts.

The differences between the measurement and simulation responses shown in Fig. 10 are mainly caused by imperfections in connection and fabrication, which can generate reactive or dispersive components in the measurement system [2], [4]. Since these imperfections are not captured by simulation, their results have a better correlation with calculations than measurements, especially in higher frequencies which are more influenced by undesired reactive components and losses [18].

The simulation time of a 2-meters anchor rod can take about 96 minutes while the proposed method reached almost the same result in about 6 seconds, as shown in Table II. The simulation times of MDSC and the end section of the transmission line (Fig. 9) are not considered to estimate the performance of the proposed method, since these results are obtained only once for almost all conditions of anchor rod, and it will not be necessary to simulate them again.

The results in Fig. 10 show that a faulty rod may have more resonant frequencies than a faultless rod. However, as the position and size of the fault can influence the resonance pattern, a machine learning

analysis is necessary to diagnose a varied set of rods [14].

For the field setup, the results of the proposed method also present a better correlation in lower frequencies. Fig. 11 and Fig. 12 present the responses of measurement, simulation and calculation from faultless 6-meter and 9-meter anchor rods connected to MDSC up to (a) 120 MHz and (b) 20 MHz.

The frequency range of 120 MHz was chosen because it contains most part of the signal energy. A better correlation between measurement and modeling was observed for the frequency range limited to 20 MHz. In this case, the difference between the measured and modeled signals are even greater at higher frequencies due to the presence of the soil.

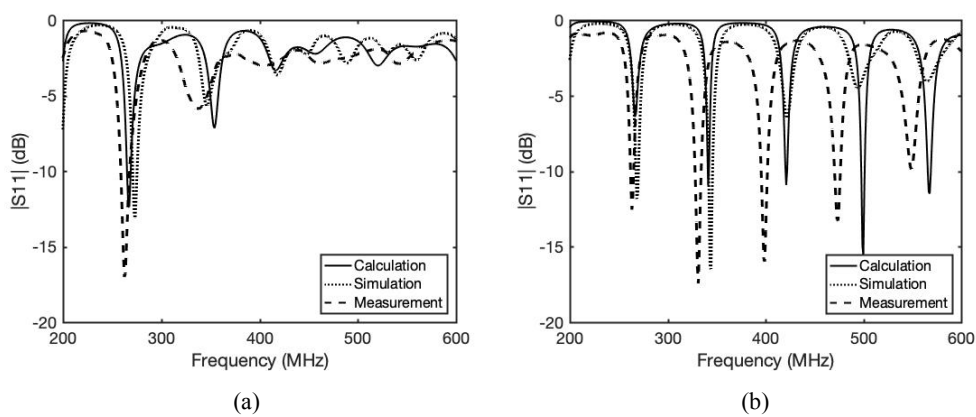


Fig. 10. Laboratory setup: measurement, simulation and calculation results for a 2-meter anchor. (a) faultless. (b) faulty.

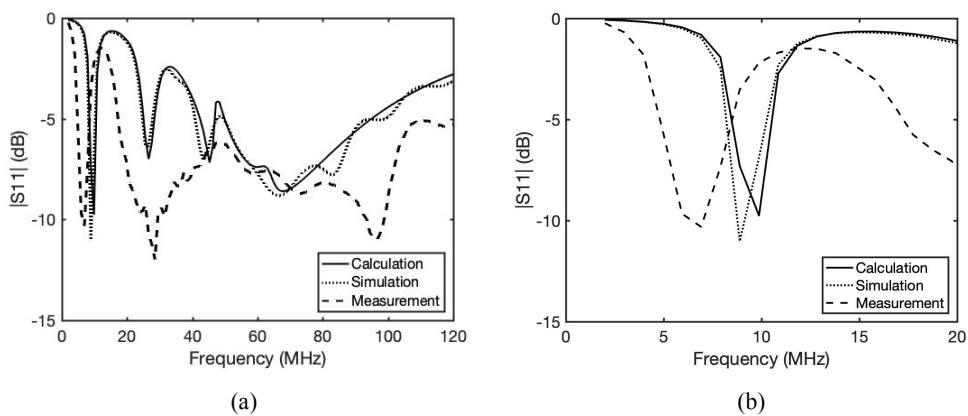


Fig. 11. Field setup: measurement, simulation, and calculation results for a faultless 6-meter anchor rod up to (a) 120 MHz and (b) 20 MHz.

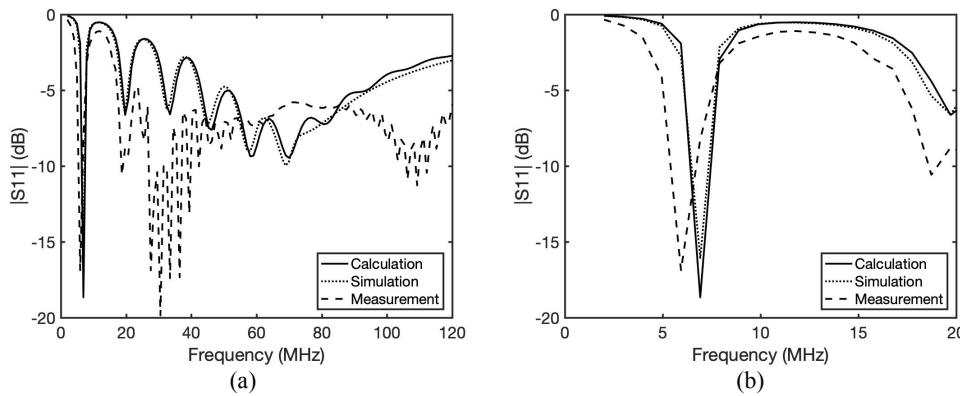


Fig. 12. Field setup: measurement, simulation, and calculation results for a faultless 9-meter anchor rod up to (a) 120 MHz and (b) 20 MHz.

Looking at the frequency range up to 20 MHz, it is noted that the resonant frequency for a 6-meter rod tends to be higher than the resonant frequency for a 9-meter rod. This is to be expected, as longer-length transmission lines generate lower resonant frequencies [18]. The 6-meter rod simulation takes over 65 minutes while the simulation without MDSC only lasted 9 minutes. For the 9-meter rod, the complete simulation takes over 83 minutes while the same simulation without the MDSC only lasted 14 minutes. Table II presents the Pearson correlation, time spent, and computational processes of the obtained results related to four anchor configurations.

TABLE II. PEARSON CORRELATION, TIME SPENT AND COMPUTATIONAL PROCESSES OF THE RESULTS

Anchor Configuration	Method	Correlation with Finite Element Simulation Signal	Correlation with Experimental Measurement Signal	Estimated time spent	Amount of Elements Required by Simulation
2.0 m faultless rod Fig. 10 (a)	Matrix ABCD Calculation (proposed)	85.70%	86.62%	6 seconds	0
	Finite Element Simulation (HFSS Software)	100.0%	97.07%	4200 seconds	81651
2.0 m faulty rod Fig. 10 (b)	Matrix ABCD Calculation (proposed)	98.84%	73.03%	6 seconds	0
	Finite Element Simulation (HFSS Software)	100.0%	74.72%	5760 seconds	90124
6.0 m faultless rod Fig. 11	Matrix ABCD Calculation (proposed)	97.11%	(a) 69.87% (b) 81.73%	540 seconds	8517
	Finite Element Simulation (HFSS Software)	100.0%	(a) 65.58% (b) 82.80%	3900 seconds	77414
9.0 m faultless rod Fig. 12	Matrix ABCD Calculation (proposed)	98.30%	(a) 64.92% (b) 88.33%	840 seconds	12007
	Finite Element Simulation (HFSS Software)	100.0%	(a) 62.04% (b) 90.10%	4980 seconds	84426

The hardware setup used was an Intel® Xeon® CPU (E5-2660 v4 2 GHz) with 128 GB of RAM memory. Therefore, insert MDSC response mathematically with the proposed method can save time and computer processing efforts, as desired.

Ansys HFSS uses Finite Element Method. The exact number of solved elements in each simulation is related to the software method solver. The simulation time is not a very precise parameter, since it can vary depending on the computer hardware, but the number of solved elements tends to be the same regardless of the hardware. Table II presents the number of elements for the 6-meter and 9-

meter rods in the field setup to be less than those for a 2-meter rod in the laboratory setup, as long as there is the presence of MDSC in both. For this, a 2-meter rod are closer in size to the MDSC, so the EM software is able to divide the 3D model into more elements, especially in the MDSC vicinity [9].

Table II also presents the percentages obtained by Pearson's correlation between calculated, simulated and measured results from Fig. 10, Fig. 11 and Fig. 12 which quantifies the degree of linear correlation between these quantities [20]. These results corroborate the obtained visualization with correlations ranging from 85.70 to 98.84% between calculations and simulations, and 69.87 to 86.82% for calculations and measurements.

From the results, it can be observed that the proposed method presents similar performance to traditional tools in modelling the real field configuration of the anchor rod but requiring significantly less computational time to obtain the responses.

The modeling of the laboratory setup presented better correlation results as compared to the field setup. In fact, it was not possible to entirely model the soil for the field setup, as it contains unknown layers composed by different minerals and organic materials. Nevertheless, the field setup modeling reached a correlation greater than 80% in the frequency range up to 20 MHz.

IV. CONCLUSIONS

The results obtained through the proposed methodology show that the electromagnetic modelling of cable-stayed towers anchoring of electric power transmission lines can be optimized by using the ABCD matrix multiplication method, known as cascade analysis, and obtaining the S-parameters through computational simulation of complex structures such as the MDSC connector.

The signals obtained with the proposed approach presented levels of correlation greater than 85% in comparison with traditional simulation tools, and similar performances in modelling real anchor rods. Moreover, the computational time required to obtain the response of the anchor rod model was from 7 to 960 times faster than by the traditional finite element approach.

The methodology used conventional programming routines, reducing, or even eliminating the computational efforts of 3D electromagnetic simulation software, and thus optimizing the time required to obtain the results. The proposed methodology proved to be applicable for non-uniform transmission lines even for those whose propagation medium is soil. Therefore, the results obtained can be used to build an expressive database which enables the development of a machine learning-based system for detecting structural faults on the anchor rods. Electricity transmission companies which use cable-stayed towers could use such a system in their maintenance routines in order to reduce costs and mitigate risks, which are quite high when using traditional methods of analysis by excavation and visual inspection.

ACKNOWLEDGMENT

This paper is the result of a R&D project developed by the institutions UFPE - Universidade Federal de Pernambuco, and IATI - Instituto Avançado de Tecnologia e Inovação, to the company Brazilian Microwave and Optoelectronics Society-SBMO received 30 June 2021; for review 9 July 2021; accepted 11 Nov 2021
Brazilian Society of Electromagnetism-SBMag © 2022 SBMO/SBMag



Sistema de Transmissão Nordeste S.A. - STN, linked to the Research and Development Program of the Electric Sector Brazilian, and sponsored by the Brazilian regulatory agency for the electric energy ANEEL - Agência Nacional de Energia Elétrica.

REFERENCES

- [1] J. M. B. Bezerra *et al.*, "Localization and diagnosis of stay rod of V guyed towers corrosion," in *2014 ICHVE International Conference on High Voltage Engineering and Application*, Sep. 2014, pp. 1–5, doi: 10.1109/ICHVE.2014.7035402.
- [2] M. S. Coutinho *et al.*, "Machine learning-based system for fault detection on anchor rods of cable-stayed power transmission towers," *Electr. Power Syst. Res.*, vol. 194, p. 107106, May 2021, doi: 10.1016/j.epsr.2021.107106.
- [3] D. C. P. Barbosa *et al.*, "Machine Learning Approach to Detect Faults in Anchor Rods of Power Transmission Lines," *IEEE Antennas Wirel. Propag. Lett.*, vol. 18, no. 11, pp. 2335–2339, Nov. 2019, doi: 10.1109/LAWP.2019.2932052.
- [4] D. C. P. Barbosa *et al.*, "An electromagnetic multi-parameter strategy to detect faults in anchor rods using neural networks," in *2019 IEEE - SBMO International Microwave and Optoelectronics Conference (IMOC)*, 2019, doi: 10.1109/IMOC43827.2019.9317602
- [5] M. M. Alves *et al.*, "Nondestructive Inspection of Anchor Rods based on Frequency Domain Reflectometry," in *2019 IEEE - SBMO International Microwave and Optoelectronics Conference (IMOC)*, 2019, doi: 10.1109/IMOC43827.2019.9317679
- [6] M. D. S. Coutinho *et al.*, "A Novel Methodology to Detect Faults on Anchor Rods Using Reflectometry and Machine Learning," in *2019 IEEE - SBMO International Microwave and Optoelectronics Conference (IMOC)*, 2019, doi: 10.1109/IMOC43827.2019.9317671
- [7] M. M. Alves *et al.*, "A novel iterative method to estimate the soil complex permittivity from measurement and simulation modeling," in *2021 IEEE Radio and Wireless Symposium (RWS)*, Jan. 2021, pp. 76–79, doi: 10.1109/RWS50353.2021.9360397.
- [8] W. T. Wang, B. M. W. Tsui, E. C. Frey, and D. E. Wessell, "Comparison of an analytical and an iterative based collimator-detector response compensation method in SPECT," in *1998 IEEE Nuclear Science Symposium Conference Record. 1998 IEEE Nuclear Science Symposium and Medical Imaging Conference (Cat. No.98CH36255)*, vol. 2, pp. 1382–1386, doi: 10.1109/NSSMIC.1998.774410.
- [9] Y. Watanabe, Y. Sato, and H. Igarashi, "Performance of 3-D infinite elements for high-frequency electromagnetic fields," *IEEE Trans. Magn.*, vol. 49, no. 5, pp. 1673–1676, 2013, doi: 10.1109/TMAG.2013.2240281.
- [10] H. V. H. S. Filho *et al.*, "Design of a connector for fault detection in eye bolts used as insulator anchorages," *Eng. Res. Express*, vol. 2, no. 4, p. 045021, Nov. 2020, doi: 10.1088/2631-8695/abc9d0.
- [11] E. J. P. Santos and L. B. M. Silva, "Calculation of scattering parameters in multiple-interface transmission-line transducers," *MEASUREMENT*, vol. 47, pp. 248–254, 2014, doi: 10.1016/j.measurement.2013.08.024.
- [12] L. Sommervogel, "Various models for faults in transmission lines and their detection using time domain reflectometry," *Prog. Electromagn. Res. C*, vol. 103, no. April, pp. 123–135, 2020, doi: 10.2528/pierc20040706.
- [13] V. L. Tarrago *et al.*, "Modelagem eletromagnética da ancoragem de torres transmissoras de energia elétrica," in *19th Simpósio Brasileiro de Micro-ondas e Optoeletrônica and 14th Congresso Brasileiro de Eletromagnetismo (MOMAG)*, 2020.
- [14] D. C. P. Barbosa *et al.*, "Artificial Neural Network-Based System for Location of Structural Faults on Anchor Rods Using Input Impedance Response," *IEEE Transactions on Magnetics*, vol. 57, no. 7, p. 62005004, July 2021, doi: 10.1109/TMAG.2021.3076013.
- [15] C. P. Costa, A. G. D'Assunção, H. C. Nascimento, and A. G. D'Assunção Junior, "Simulation and design of a bandpass filter based on substrate integrated e-plane waveguide," *J. Microwaves, Optoelectron. Electromagn. Appl.*, vol. 18, no. 3, pp. 390–398, 2019, doi: 10.1590/2179-10742019v18i31552.
- [16] M. J. Duarte, V. P. Da Silva Neto, and A. G. D'Assunção, "Synthesis and mechanical reconfiguration of ground plane tilted microstrip antennas based on tetra-circle fractals," *J. Microwaves, Optoelectron. Electromagn. Appl.*, vol. 19, no. 2, pp. 228–241, 2020, doi: 10.1590/2179-10742020v19i2838.
- [17] A. M. Lima, J. V. de Freitas, and O. P. Lavor, "Analysis of the Resonator Element in Different Positions in the Circular Patch Microstrip Antenna," *J. Microwaves, Optoelectron. Electromagn. Appl.*, vol. 20, no. 1, pp. 16–29, Mar. 2021, doi: 10.1590/2179-10742021v20i1954.
- [18] D. M. Pozar, *Microwave Engineering*, 4th ed. John Wiley & Sons, 2012.
- [19] W. Liu, "Electromagnetic Modeling of Embedded Metallic Structures for Nondestructive Evaluation Using Time Domain Reflectometry," University of Delaware, 2001.
- [20] H. Xu and Y. Deng, "Dependent Evidence Combination Based on Shearman Coefficient and Pearson Coefficient," *IEEE Access*, vol. 6, pp. 11634–11640, 2018, doi: 10.1109/ACCESS.2017.2783320.